†Electronic Supplementary Information

Phase diagram and oxygen-vacancy ordering in the $CeO_2-Gd_2O_3$ system: A theoretical study

Pjotrs A. Žguns,*[ab] Andrei V. Ruban,[bc] and Natalia V. Skorodumova[ab]

[a] *Department of Physics and Astronomy, Uppsala University, Box 516, 75121 Uppsala, Sweden. E-mail: pjotr.zgun@gmail.com*
[b] *Department of Materials Science and Engineering, KTH Royal Institute of Technology, 10044 Stockholm, Sweden*
[c] *Materials Center Leoben Forschung GmbH, A-8700 Leoben, Austria*

1.a Crystal structure of CeO_2 and C-type Gd_2O_3

The description of fluorite CeO_2 and C-type Gd_2O_3 structures is given in Table S.1. Fluorite CeO_2 can be represented in the frames of both *Fm-3m* and *Ia-3* space groups, while C-type Gd_2O_3 in the frame of *Ia-3* space group only. C-type Gd_2O_3 and fluorite CeO_2 lattices coincide if $x(\mathrm{M2}) = 0$, $x(\mathrm{O1}) = \frac{3}{8}$, $y(\mathrm{O1}) = \frac{1}{8}$, $z(\mathrm{O1}) = \frac{3}{8}$, and $x(\mathrm{O2}) = \frac{3}{8}$. In the C-type Gd_2O_3 $x(\mathrm{M2}) \approx -0.03$, $x(\mathrm{O1}) \approx 0.39$, $y(\mathrm{O1}) \approx 0.15$, $z(\mathrm{O1}) \approx 0.38$ (Scavini *et al.*, IUCrJ, **2**, 511-522, 2015).

If the configuration of vacancies in $Ce_{1-x}Gd_xO_{2-x/2}$ is random, then O2 site occupation $Y(\mathrm{O2}) = 1 - 0.25x_{\mathrm{Gd}}$. If the configuration of vacancies in $Ce_{1-x}Gd_xO_{2-x/2}$ has the C-type order, then $Y(\mathrm{O2}) = 1 - x_{\mathrm{Gd}}$.

Table S.1 Table showing a connection between fluorite (CeO_2) and C-type (Gd_2O_3) structures. C-type Gd_2O_3 unit cell (*cI80*) can be seen as $2\times2\times2$ unit cell of CeO_2 (*cF12*). Adopted from Coduri *et al.*, *Phys. Chem. Chem. Phys.* **19**, 11612-11630, 2017.

Label	CeO_2 fluorite (*Fm-3m*, *cF12*)	CeO_2 Fluorite (*Ia-3*, *cI96* setting)	C-type Gd_2O_3 (*Ia-3*, *cI80*)
M1	4a $(0,0,0)$	8b $(\frac{1}{4},\frac{1}{4},\frac{1}{4})$	8b $(\frac{1}{4},\frac{1}{4},\frac{1}{4})$
M2	$\equiv$ M1	24d $(0,0,\frac{1}{4})$	24d $(x,0,\frac{1}{4})$
O1	8c $(\frac{1}{4},\frac{1}{4},\frac{1}{4})$	48e $(\frac{3}{8},\frac{1}{8},\frac{3}{8})$	48e (x,y,z)
O2	$\equiv$ O1	16c $(\frac{3}{8},\frac{3}{8},\frac{3}{8})$	16c (x,x,x) (empty)

1.b Calculated structures (DFT)

We have calculated the various sets of structures as described in Table S.2 and below.

Table S.2 The DFT-calculated sets of structures with different supercell sizes and Gd concentrations. Sets were used for calculation of cluster interactions (CIs), validation of CIs and analysis of how C-type Va order affects structural parameters. Sets '_above' and '_below' have Va configurations similar to those respectively *above* and *below* the Va ordering temperature in the quenched cations system ($T^{\mathrm{q}}_{\mathrm{ord}}$), and therefore have different O2 site occupations ($Y(\mathrm{O2})$). *Above* $4\times4\times4$ structures were chosen similar to those $12\times12\times12$ at 1500 K ($x_{\mathrm{Gd}} = 0.3750$), 2000 K ($x_{\mathrm{Gd}} = 0.4375,\ 0.5000$) or 3000 K ($x_{\mathrm{Gd}} = 0.7500$). *Below* $4\times4\times4$ structures were chosen similar to those $12\times12\times12$ at 500 K ($x_{\mathrm{Gd}} = 0.3750,\ 0.4375,\ 0.5000,\ 0.7500$). The outcome O2 site occupations are shown (the range and structure-averaged value). For set 08–11, each structure was calculated for 6 cubic lattice parameters ($a(cF12) = 5.3375,\ 5.3625,\ 5.3875,\ 5.4125,\ 5.4375,\ 5.4700$). Sets set_01 and set_04 were calculated in our previous work (Žguns *et al.*, *Phys. Chem. Chem. Phys.*, 2017, **19**, 26606-26620).

Set	Supercell	x_{Gd}	$N_{\mathrm{struct.}}$	$a(cF12)$ (Å)	Used for	$Y(\mathrm{O2})$ range	$\langle Y(\mathrm{O2})\rangle_{\mathrm{str}}$	Comment
01	$3\times3\times3$	0.1296	210	5.4700	CE			
02	$3\times3\times3$	0.5000	172	5.4700	CE			
03	$3\times3\times3$	0.8704	145	5.4700	CE			
04	$4\times4\times4$	0.1250	168	5.4700	CE			
05	$4\times4\times4$	0.0625	10	5.4700	validation			
06	$4\times4\times4$	0.5000	10	5.4700	validation			
07	$4\times4\times4$	0.8750	12	5.4700	validation			
08_below	$4\times4\times4$	0.3750	9	5.3375, ..., 5.4700	str. param.	0.63-0.65	0.63	C-type Va order
08_above	$4\times4\times4$	0.3750	9	5.3375, ..., 5.4700	str. param.	0.66-0.80	0.73	rnd.-like Va conf.
09_below	$4\times4\times4$	0.4375	7	5.3375, ..., 5.4700	str. param.	0.56-0.57	0.57	C-type Va order
09_above	$4\times4\times4$	0.4375	7	5.3375, ..., 5.4700	str. param.	0.73-0.83	0.78	rnd.-like Va conf.
10_below	$4\times4\times4$	0.5000	3	5.3375, ..., 5.4700	str. param.	0.50	0.50	C-type Va order
10_above	$4\times4\times4$	0.5000	2	5.3375, ..., 5.4700	str. param.	0.72	0.72	rnd.-like Va conf.
11_below	$4\times4\times4$	0.7500	7	5.3375, ..., 5.4700	str. param.	0.25	0.25	C-type Va order
11_above	$4\times4\times4$	0.7500	3	5.3375, ..., 5.4700	str. param.	0.62-0.72	0.67	rnd.-like Va conf.

Sets '_above' and '_below' have Va configurations similar to those respectively *above* and *below* the Va ordering temperature in the quenched cations system ($T^{\mathrm{q}}_{\mathrm{ord}}$). Although the random-like (*above*) configurations were not modelled perfectly, they differ from the C-type ordered (*below*) configurations, as the $Y(\mathrm{O2})$ site occupation shows. These configurations (sets 08–11) were used for calculations of structural parameters (see Section 5 in the paper). Each structure in _above set has its counterpart in _below set with exactly the same (random) configuration of cations. The number of structures in _above sets is sometimes smaller than in _below sets, since relaxation of high-energy configurations was problematic: i) for some configurations forces acting on atoms where $\gg 0.01$ eV/Å; ii) migration of O^{2-} can occur, decreasing the energy (thus initial structure is not preserved). Both i) and ii) structures where not considered, unless

stated explicitly. For sets 8–11, structures were calculated for $a = 5.3375, ..., 5.4700$ Å, in order to calculate the equilibrium cubic lattice constant by fitting E *vs.* a data with Birch-Murnaghan equation of state.

1.c Deviations from ideal fluorite structure

Here we analyse how CGO ($Ce_{1-x}Gd_xO_{2-x/2}$) structure changes with concentration ($x_{Gd} = 0.13, 0.50, 0.87$). We consider $3 \times 3 \times 3$ supercells (324 lattice sites). In most of the considered supercells the configuration of Gd and Va is quite random. We average the pair distribution function (PDF) over 40 supercells. PDFs are shown in Fig. S.1. Even for small Gd concentration the interatomic distances deviate from those of the ideal fluorite. Some split into long and short. For example, the cation-cation nearest neighbour distance in the fluorite structure splits into short and long ones, similar to C-type Gd_2O_3. In general, broadening of peaks, their splitting and merging become more pronounced with increasing Gd concentration. (Note that for all these structures, after geometry optimisation was performed, we could unambiguously map each atom to corresponding fluorite lattice sites. This gives us the ground to use the fluorite lattice in the cluster expansion scheme.)

1.d Concentration dependence of cluster interactions

Here we analyse the change of cluster interactions (CIs) with concentration. The CIs for $x_{Gd} = 0.13$ where determined previously (see ref.[1]), while here we determine CIs for $x_{Gd} = 0.50, 0.87$. The shape of curves is very much the same (see Fig. S.2). Next, we note that for larger concentrations ($x_{Gd} = 0.50, 0.87$) the ΔJ are much larger, as compared to $x_{Gd} = 0.13$ This reflects the change in local structure, as seen by PDF (see Fig. S.1), *i.e.* more pronounced peaks' broadening and splitting at higher concentrations.

Regarding the trends in concentration dependence of CIs, in general CIs at $x_{Gd} = 0.50$ are ca 0.04 eV larger than CIs at $x_{Gd} = 0.13$ (Fig. S.2). For CIs at $x_{Gd} = 0.87$ there is no uniform trend, they show significant scatter. The shape of CI-curves for Va−Va and Gd−Va are quite concentration independent.

1.e Finite size effects in defects' ordering

The considered supercells ($4 \times 4 \times 4$) can accommodate both the C-type Va order and random configuration of vacancies. The short range order parameters are very much the same as observed in larger supercells (*e.g.* $12 \times 12 \times 12$). Therefore $4 \times 4 \times 4$ supercells can be used in DFT calculations to study the effect of Va ordering on the structural parameters. Also the O−Va ordering transition, occurring at high temperatures, is captured in MC simulations using $4 \times 4 \times 4$ supercells, and energies of structures across transitin are predicted well (see Fig. 1 in the paper, $x_{Gd} = 0.500$, 0.875).

As for the phase separation, occurring at lower temperatures, it includes clustering of cations. Occasionally, much larger supercells are required, like $8 \times 8 \times 8$, in order to reproduce SRO parameters correctly (as they are in $12 \times 12 \times 12$ supercells). The $4 \times 4 \times 4$ supercells reproduce somewhat different short range order at lower temperatures. Nevertheless, we believe that for this test (Fig. 1 in the paper) it is not crucial whether actual short range order corresponds exactly to that in larger MC supercells. The most important is the comparison of DFT and CE energies itself.

1.f Comparison of configurational energies: CE *vs.* DFT

Fig. S.3 shows the comparison between DFT and CE calculated configurational energies for $x_{Gd} = 0.50, 0.87$ ($3 \times 3 \times 3$ supercells). CE energies were predicted using CIs determined for $x_{Gd} = 0.125$.

1.g Effect of point defects' configuration on electronic structure and Bader charges

Here we consider the effect of point defects's redistribution on the electronic structure and ionic charges. We analyse three concentrations ($x_{Gd} = 0.0625, 0.5000, 0.8750$) and consider structures encountered in Monte Carlo simulations with different degree of ordering corresponding to different temperatures (see Section 2.4 in the main paper). As one can see from Fig. S.4, redistribution of point defects (Gd and Va) in the bulk affects the width of the band gap and shape of the Density of States (DOS) of CGO ($Ce_{1-x}Gd_xO_{2-x/2}$). However, it seems that these changes do not influence bonding much, as cluster interactions used ($x_{Gd} = 0.125$) can reproduce the configurational energy quite well (see Fig. 1 in the main paper). Perhaps, the most crucial is that we do not observe a gap closing, *i.e.* CGO remains ionic. We also observe that the redistribution of point defects does not influence the Bader charges much either (see Fig. S.5).

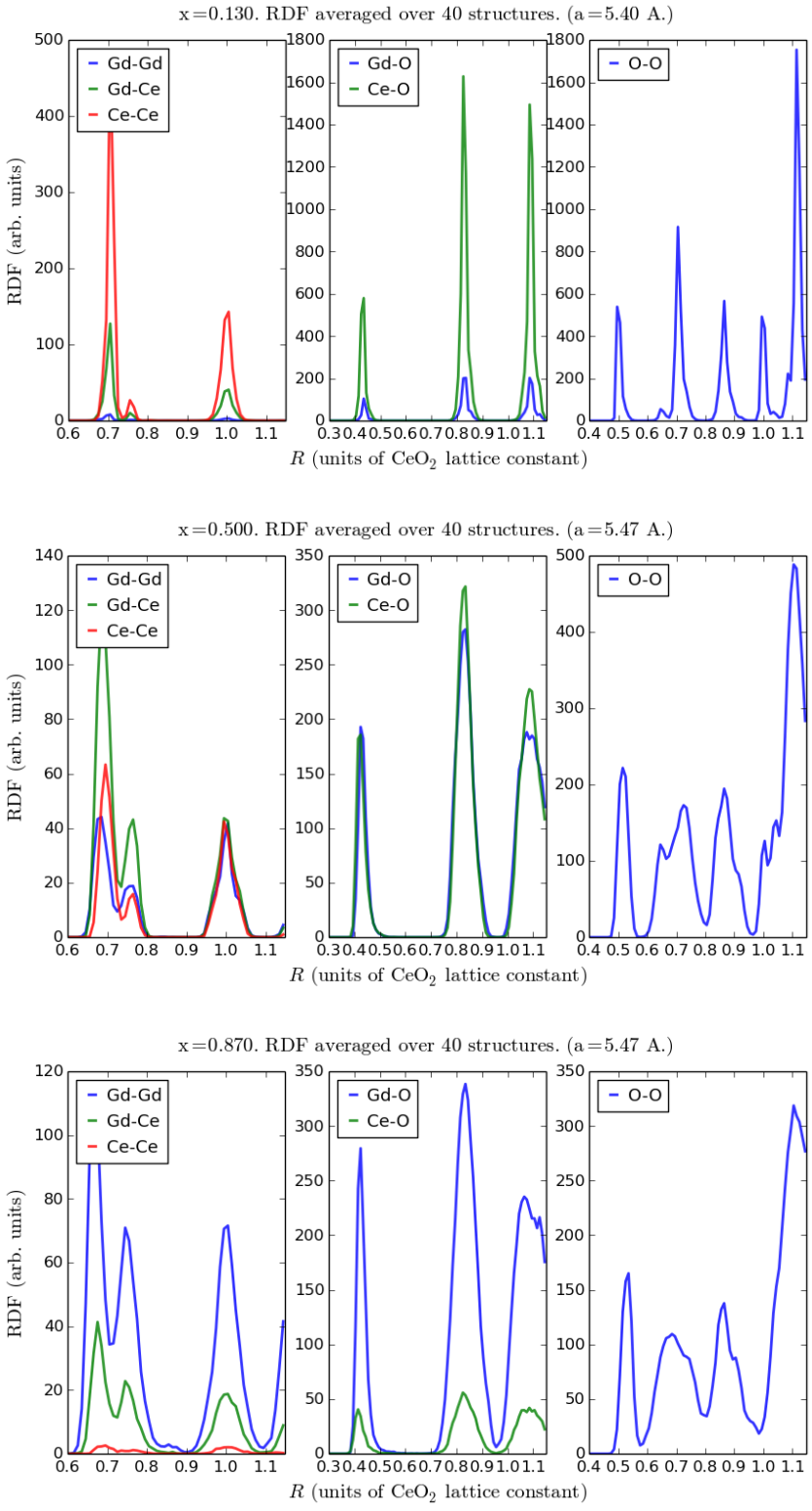

Fig. S.1 PDF for $x_{\mathrm{Gd}} = 0.13, 0.50, 0.87$ (averaged over 40 structures). Upon increase of concentration PDF peaks becomes broader and some of them merge.

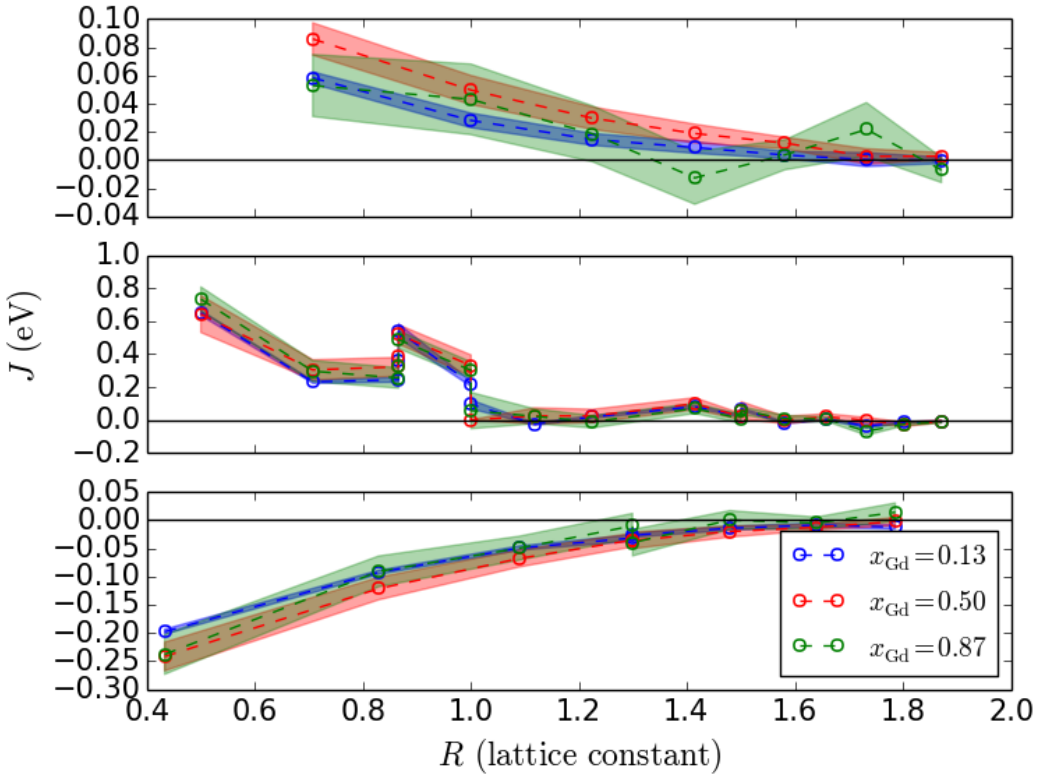

Fig. S.2 CIs for $x_{\mathrm{Gd}} = 0.13, 0.50, 0.87$ ($a = 5.47$ Å). The colour fillings show the standard errors of CIs (ΔJ) as found from 1000 trial CE, each done with 100 structures randomly chosen from the larger sets (210, 172, 149 structures for, $x_{\mathrm{Gd}} = 0.13, 0.50, 0.87$, respectively).

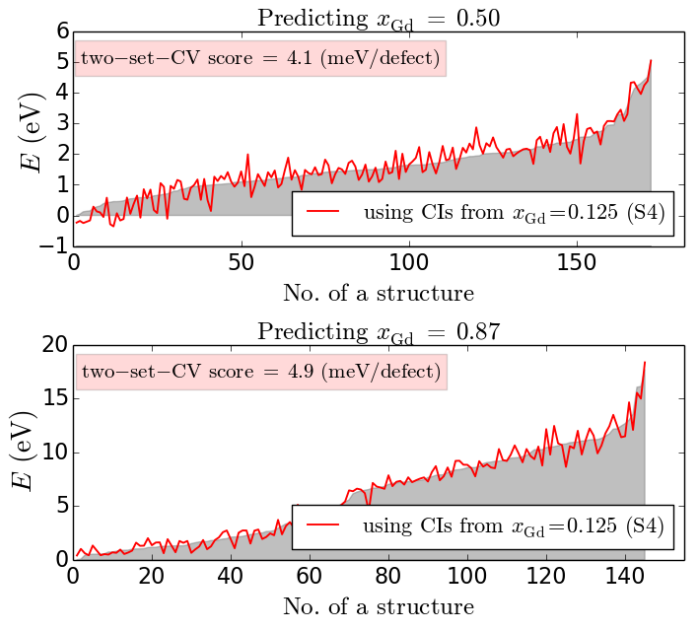

Fig. S.3 *E vs.* no. of a structure. Comparing E_{DFT} (grey filling) and E_{CE} (red lines) for $x_{\mathrm{Gd}} = 0.50, 0.87$. E_{CE} is predicted using CIs determined for $x_{\mathrm{Gd}} = 0.125$.

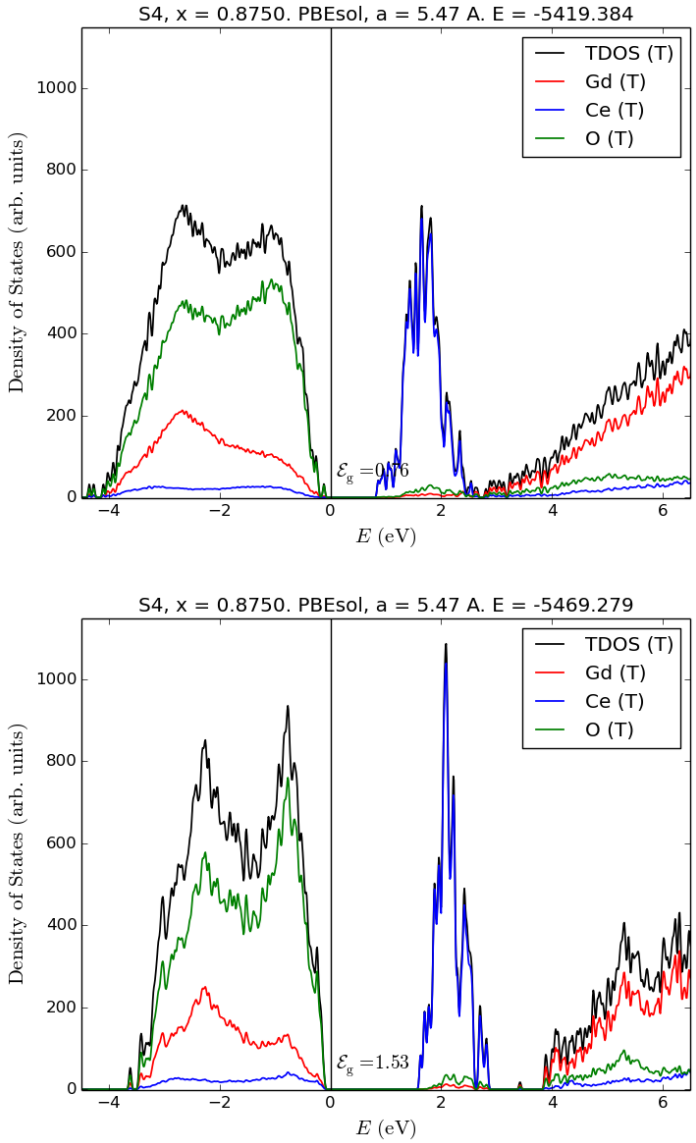

Fig. S.4 Density of States (DOS) of the high energy configuration (top) and low energy configuration (bottom) for $x_{\mathrm{Gd}} = 0.8750$ (correspond to highest E and lowest E points in the bottom panel of Fig. 1 in the paper).

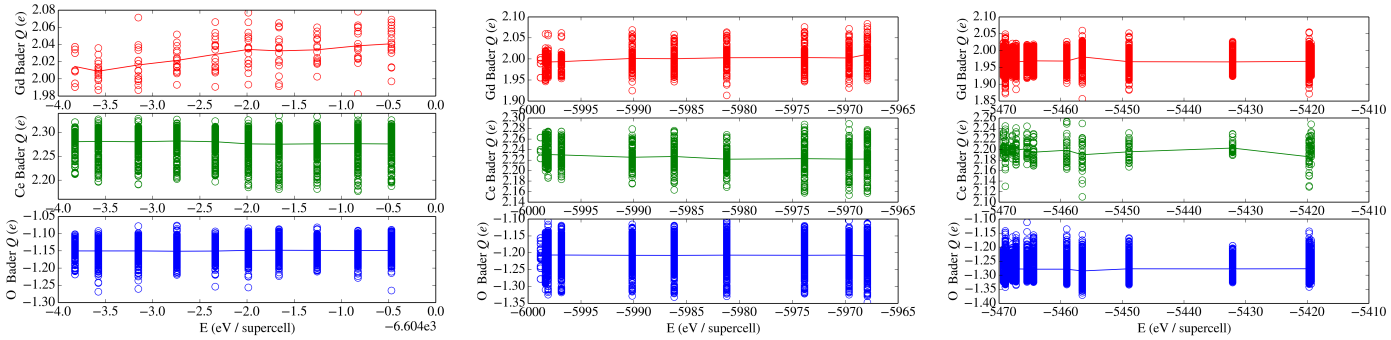

Fig. S.5 The scatter of Bader charges of Gd, Ce and O *vs.* supercell energy for $x_{\mathrm{Gd}} = 0.0625, 0.5000, 0.8750$ (from left to right, respectively). Solid lines show averages.

1.h Calculation of oxygen O2 site occupation, $Y(\mathrm{O2})$

As mentioned in the paper, to calculate $Y(\mathrm{O2})$, we considered all possible O2 site Wyckoff positions in the oxygen-vacancy simple cubic lattice in the MC supercell. The minimal $Y(\mathrm{O2})$ value was chosen among those obtained.

Indeed, if the Va configuration is essentially random, then $Y(\mathrm{O2}) \approx 1 - x_{\mathrm{Gd}}/4$ for any possible O2 site Wyckoff position (in the supercell). However, if $Y(\mathrm{O2}) \approx 1 - x_{\mathrm{Gd}}$ for at least one O2 site Wyckoff position, then some C-type anion order is present. This conclusion is rather straightforward, as O−Va sublattice is the binary system and $Y(\mathrm{O2}) \not< 1 - x_{\mathrm{Gd}}$. Note that there are many Va configurations (in the MC supercell), which yield the same $Y(\mathrm{O2}) = 1 - x_{\mathrm{Gd}}$ (for example C-type anion order and phase separated CeO_2 and C-type Gd_2O_3). Apart from phase separation, we generally observe a rather uniform Va density in the MC supercells, therefore $Y(\mathrm{O2}) = 1 - x_{\mathrm{Gd}}$ case is called a C-type anion order.

1.g Analysis of cation relaxation pattern

In fluorite CeO_2 cations occupy the fcc sublattice. In C-type Gd_2O_3, the positions of some cations are displaced (M2 sites), as compared to these of fluorite lattice. For an arbitrary composition and configuration (DFT calculated) the relaxation pattern of cations was characterised as follows:

1) The starting point is the identification of the O2 site. Find a frame of reference yielding the minimal $Y(\mathrm{O2})$ for a given Va configuration. Thus, O2 sites are found and therefore M1, M2 sites as well.

2) The position of cation i is given by the vector: $\vec{r}_i^{\,\mathrm{F}}$ (fluorite lattice), $\vec{r}_i^{\,\mathrm{C}}$ (C-type lattice), $\vec{r}_i$ (structure under investigation).

3) Calculate displacement vectors from the fluorite lattice for the structure under investigation ($\Delta\vec{r}_i = \vec{r}_i - \vec{r}_i^{\,\mathrm{F}}$) and for the C-type lattice ($\Delta\vec{r}_i^{\,\mathrm{C}} = \vec{r}_i^{\,\mathrm{C}} - \vec{r}_i^{\,\mathrm{F}}$). Also calculate $|\Delta\vec{r}_i|$ and $|\Delta\vec{r}_i^{\,\mathrm{C}}|$.

4) Calculate misorientation angle ($\theta_{i,\mathrm{mis}}$). It is the angle between the calculated displacement vector and the reference displacement vector of C-type Gd_2O_3, *i.e.* between $\Delta\vec{r}_i$ and $\Delta\vec{r}_i^{\,\mathrm{C}}$. Since for M1 sites $\Delta\vec{r}_i^{\,\mathrm{C}} = \vec{0}$, in this case $\theta_{i,\mathrm{mis}}$ is chosen to be the angle between $\Delta\vec{r}_i$ and $\vec{e}_x \equiv \langle 1,0,0\rangle$.

Finally, we analyse the similarity to F or C structure by considering amplitudes of displacement vectors from the fluorite lattice ($|\Delta\vec{r}_i|$) and misorientation angles ($\theta_{i,\mathrm{mis}}$).

2.a Monte Carlo simulations: spatial coverage of the C-type Va order

We note that there is no unambiguous correspondence between $Y(\mathrm{O2})$ averaged over the whole MC supercell and actual Va configuration. For example, $Y(\mathrm{O2}) = 1 - x_{\mathrm{Gd}}$ corresponds to both the phase separated system (pure CeO_2 and C-type Gd_2O_3) and the C-type Va order in $Ce_{1-x}Gd_xO_{2-x/2}$. (Even though both the phase separated system and C-type Va order yield same $Y(\mathrm{O2})$, the absolute values of SRO parameters are in general larger for the phase separated system.)

In Fig. S.6, the snapshots of O−Va configurations for $x_{\mathrm{Gd}} \approx 0.75$ are shown (the Va−Va clusters of type $\langle 1,1,1 \rangle$ are shown as solid grey lines). The upper panel (Fig. S.6) shows essentially random O−Va configuration. The middle panel shows O−Va configuration below the ordering temperature. In this case there are much more Va−Va clusters of type $\langle 1,1,1 \rangle$. The bottom panel shows the phase separation into C-type Gd_2O_3 and CeO_2 (CeO_2 phase can be seen as the green 'hole' inside the C-type ordered O−Va sublattice; configurations of cations are not shown).

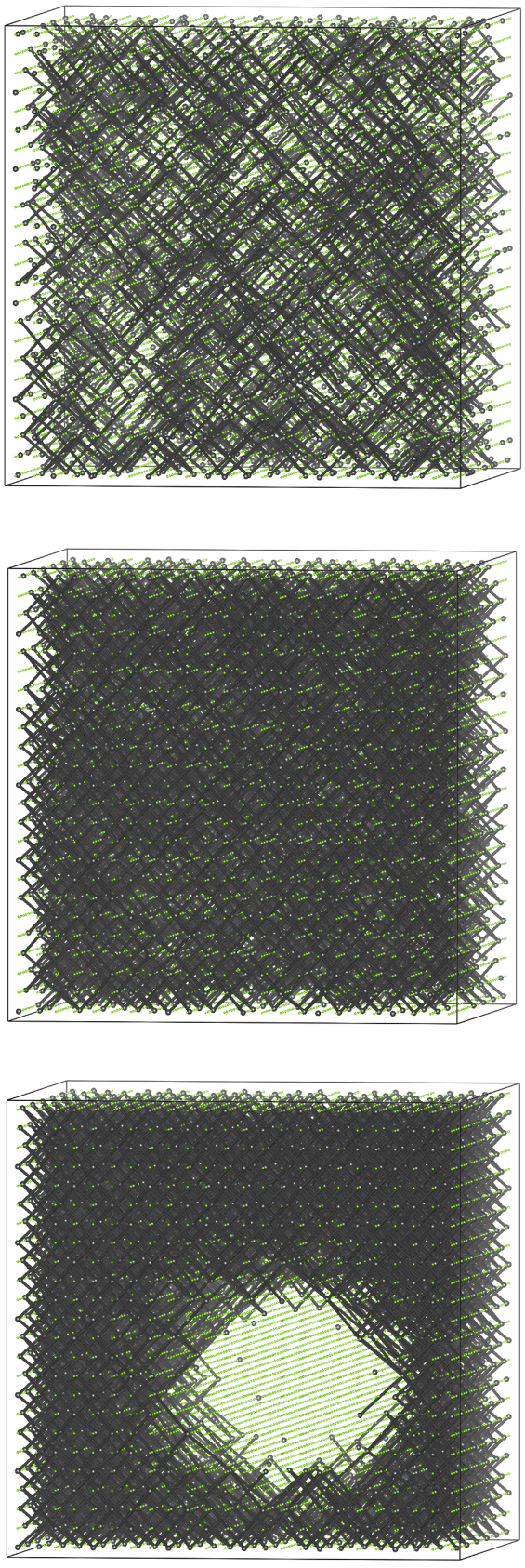

Fig. S.6 Snapshots of equilibrium distributions of O and Va on their sublattice at $T = 3000$ K ($T > T_{\mathrm{ord}} \approx 2850$ K, top row), $T = 1500$ K ($T_{\mathrm{ord}} > T > T_{\mathrm{sep}} \approx 980$ K, middle row), $T = 900$ K ($T < T_{\mathrm{sep}} \approx 980$ K, just below $T_{\mathrm{sep}} \approx 980$, bottom row). MC supercell size $12 \times 12 \times 12$ (*ca.* $65\ nm \times 65$ nm $\times 65$ nm). $x_{\mathrm{Gd}} = 0.4375$. Colour code: O — green (small), Va — grey (large). The Va$-$Va $\langle 1,1,1 \rangle$ clustering — grey lines. The Gd$-$Gd $\langle \frac{1}{2}, \frac{1}{2}, 0 \rangle$ clustering — violet lines. (Vectors are given in units of CeO_2 (*cF12*) lattice parameter.) The green 'hole' in the bottom panel correspond to the CeO_2 precipitate, which is surrounded by C-type Va ordered Gd_2O_3 phase.

2.b Contributions of Gd−Gd, Va−Va, Gd−Va pair interactions to ordering energies

Here, we analyse the contributions of different interactions to the ordering energies *vs.* x_{Gd} shown in Fig. S.7. In fact, all the pair interactions are of electrostatic origin,[1] and repulsive Va−Va interactions are the strongest among them (see ref.[1] for details). As seen in Fig. S.7, for pure Gd_2O_3 the C-type Va ordering reduces the O−Va energy. While the concentration of oxygen vacancies is high enough, ordering pattern and mechanism is 'inherited' from C-type Gd_2O_3. Indeed, the O−Va energy reduction is pronounced and remains the main driving force of the Va ordering below T_{ord} from $x_{\mathrm{Gd}} = 1$ down to $x_{\mathrm{Gd}} \approx 0.5$. At lower Gd concentrations, the Gd−Va energy reduction becomes important. As for the phase separation, it is always governed by the Gd−Va clustering.

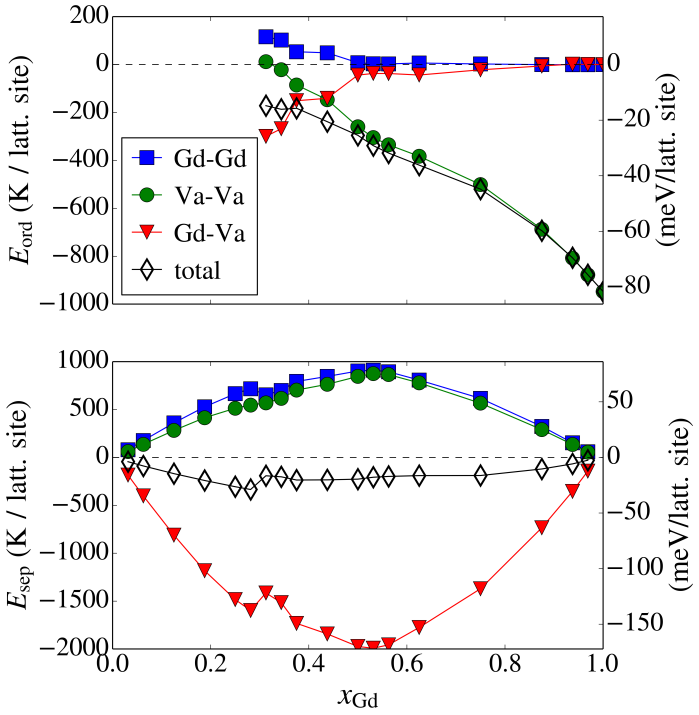

Fig. S.7 Ordering energies *vs.* x_{Gd}, calculated for the ordering transition (top) and phase separation (bottom). Top: $E_{\mathrm{ord}} = E(T^*) - E(T = 3500\ \mathrm{K})$. Bottom: $E_{\mathrm{sep}} = E(T = 200\ \mathrm{K}) - E(T^*)$. Here, T^* is a temperature in-between two transitions ($T*$ is an inflection point in the E *vs.* T curve in the $T_{\mathrm{sep}} < T^* < T_{\mathrm{ord}}$ interval). Gd−Gd, Va−Va and Gd−Va components of E_{ord} and E_{sep} are also shown. For $x_{\mathrm{Gd}} \lesssim 0.3$ there is the phase separation only, so $E_{\mathrm{ord}} \equiv 0$ and $T^* \equiv 3500$K. Note, around $x_{\mathrm{Gd}} \approx 0.3$ the partition into E_{ord} and E_{sep} is not that rigorous, because T_{ord} and T_{sep} are quite close.

2.c Monte Carlo simulations in the quenched cations systems: heat capacity *vs.* temperature

C-type Va ordering in the quenched-cations case is characterised by a wide heat capacity peak, as shown in Fig. S.8. In the thermodynamic equilibrium case, heat capacity peaks are much sharper. For $x_{\mathrm{Gd}} = 0.500$ and $x_{\mathrm{Gd}} = 0.750$, the heat capacity maximum cannot be recognised. For $x_{\mathrm{Gd}} = 0.9375$ heat capacity peak is extremely small, reflecting that rearrangements upon cooling are minor.

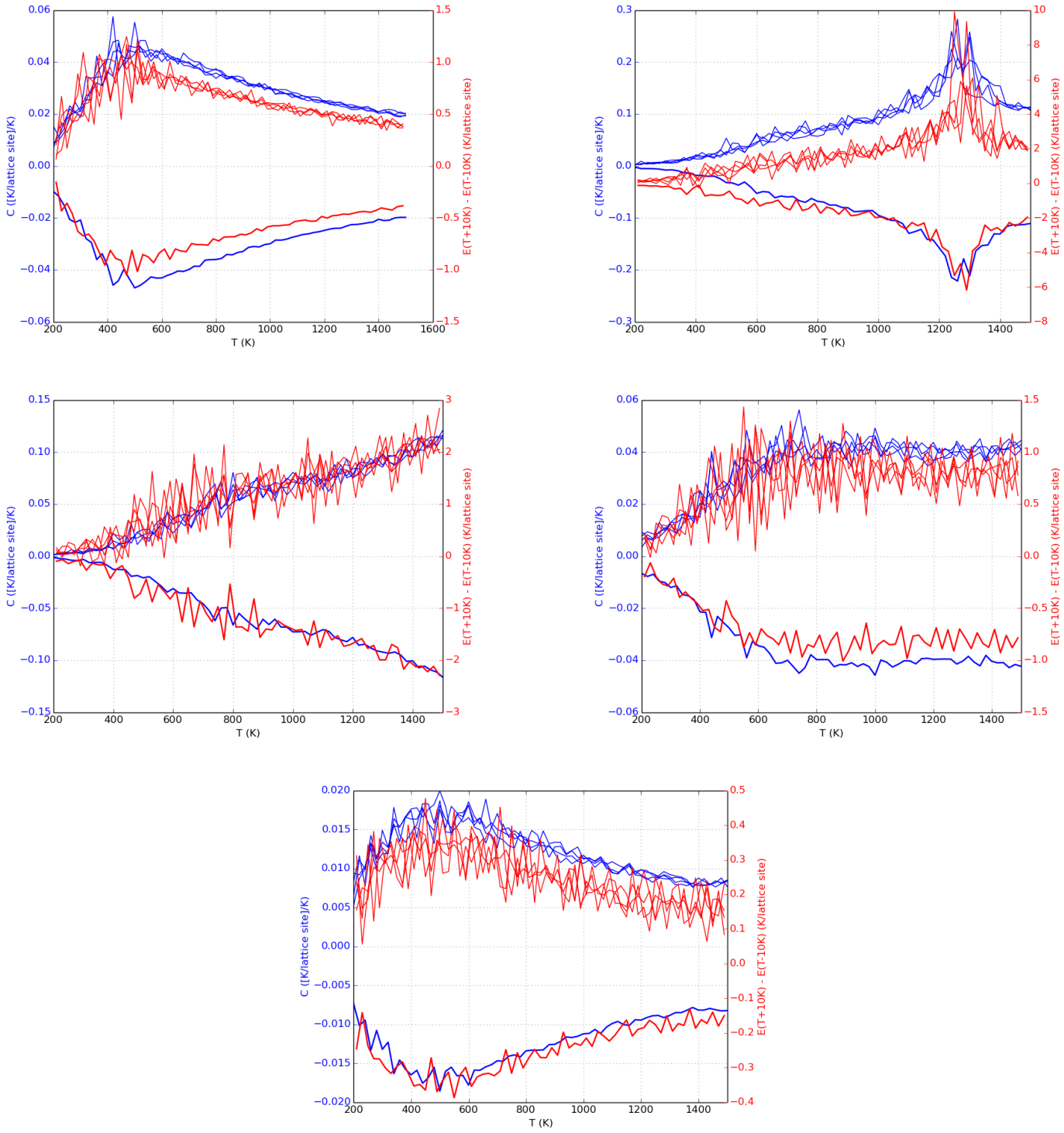

Fig. S.8 Heat capacity (blue) and energy differences (red) *vs.* temperature. Quenched cations systems. From left to right, top to bottom: $x_{\mathrm{Gd}} = 0.125, 0.375, 0.500, 0.750, 0.9375$. Averaged data is shown with minus sign (for clarity).

2.d DFT calculations of quenched structures: displacement of cations

Fig. S.9 shows displacements of cations and misorientation angles for $x_{\mathrm{Gd}} = 0.750$. Two upper figures correspond to the case *above* the ordering temperature. Two lower figures correspond to the case *below* the ordering temperature.

Fig. S.10 shows the displacements of cations *vs.* x_{Gd} for M1 and M2 cation sites.

As for the amplitudes of displacements, for the *above* structures M1 and M2 sites have very similar $|\Delta\vec{r}_i|$. For the *below* structures the amplitudes of displacements has bimodal distribution, with two peaks (Fig. S.10). One peak corresponds to small displacements with $|\Delta\vec{r}_i| = 0.01$–0.12. Second peak corresponds to large displacements with $|\Delta\vec{r}_i| = 0.12$–0.40. With increasing x_{Gd}, the M2 site cations become more similar to the M2 site cations in C-type Gd_2O_3: the peak at $|\Delta\vec{r}_i| = 0.01$–0.12 decreases, while the peak at $|\Delta\vec{r}_i| = 0.12$–0.40 grows and shits to larger values.

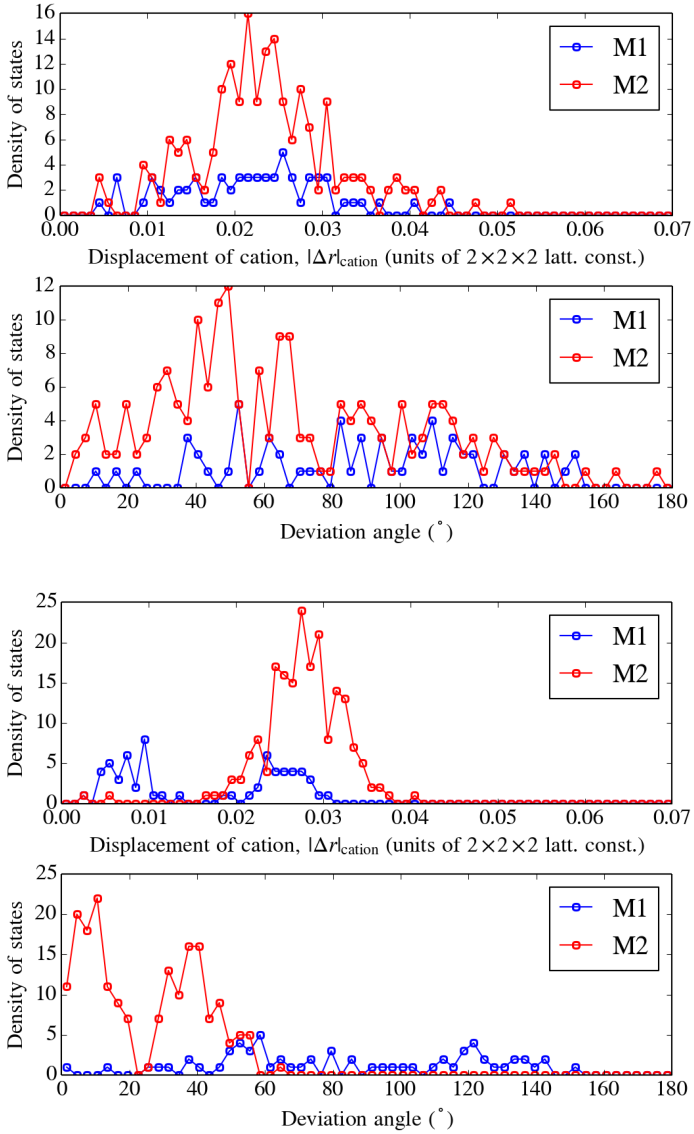

Fig. S.9 Top panel: *above* $T^{\mathrm{q}}_{\mathrm{ord}}$, $x_{\mathrm{Gd}} = 0.75$. Bottom panel: *below* $T^{\mathrm{q}}_{\mathrm{ord}}$, $x_{\mathrm{Gd}} = 0.75$. Histograms showing densities of states for: i) displacements of cations from fluorite lattice sites and ii) misorientation angles of displacement vectors with respect to the displacements in C-type Gd_2O_3 for the M2 sites, and $\vec{e}_{x=}\langle 1,0,0\rangle$ for the M1 sites.

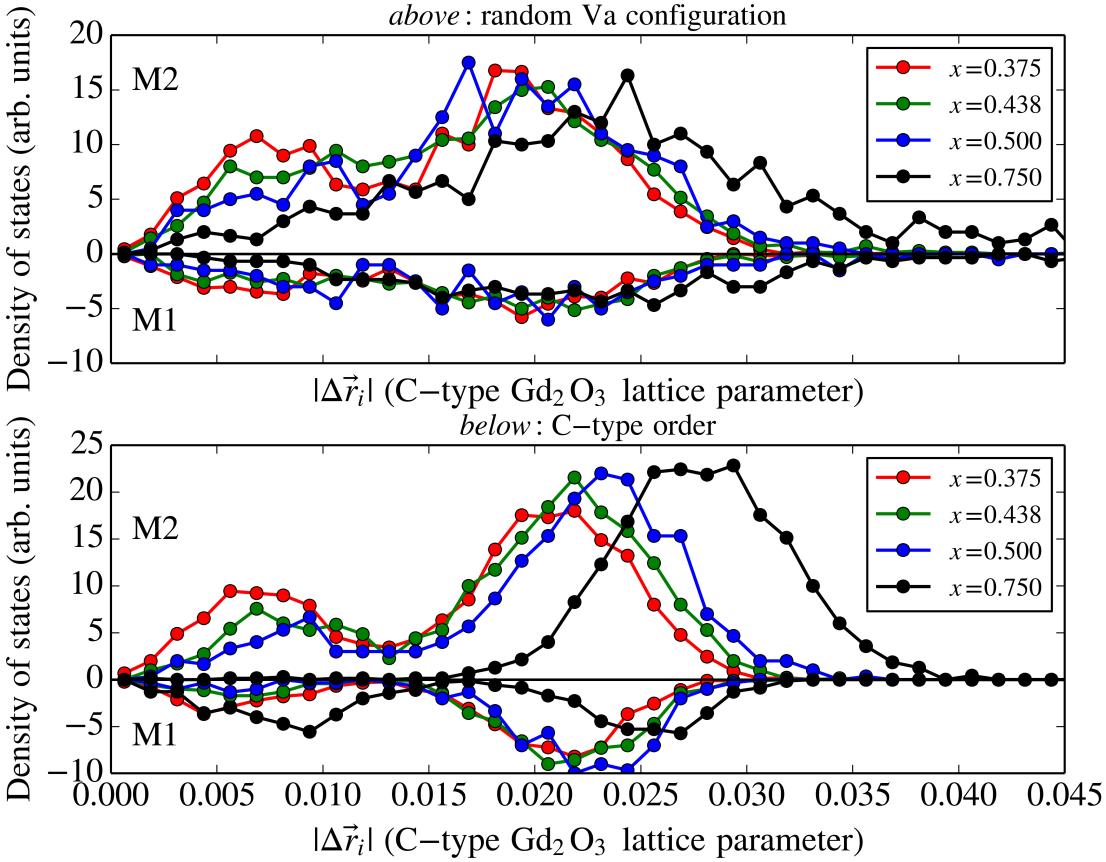

Fig. S.10 Top panel: histograms showing the densities of states of cations displacements from ideal fluorite sites ($\Delta|\vec{r}_i|$). *Above* T^{q}_{ord} and *below* T^{q}_{ord} structures are compared. For M1 site cations shown as negative densities of states (positive for M2). In C-type Gd_2O_3, $|x(\text{M2})| \approx 0.03$ and $|x(\text{M1})| = 0$.

2.e Estimation of the transition temperature from x(M2) temperature dependence

We also note that the temperature dependence of the x(M2) coordinate can be used to estimate the transition temperature between the F and C phases. As reported by Artini *et al.*,[2] at $x_{\mathrm{Gd}} = 0.3$, the x(M2) is 0.25 for 1073 K, 0.252 for 973 K, and 0.255 for 298 K (see Fig. 4 in ref.[2]; both x(M2) $= 0.00$ and $= 0.25$ correspond to the fluorite phase, depending on the choice of origin in the *Ia-3* crystallographic set-up). Thus, for $x_{\mathrm{Gd}} = 0.3$ the transition between F and hybrid C* can be at *ca.* 1000 K, which is in agreement with the calculated ordering temperature.

2.f Spatial coherence of C-phase domains

As mentioned, the CGO structure is described well only after accounting for features of both F and C phases.[2–4] Within the C* region (0.2–$0.3 \lesssim x_{\mathrm{Gd}} \lesssim 0.5$) the F and C phase domains are 'finely interlaced'.[5] Scavini with co-workers[6] report that there is a high concentration of anti-phase boundaries (APB) in the C* region, while for $x_{\mathrm{Gd}} > 0.5$ the APB concentration is very small.[6] In the Gd-rich region the alignment of cation relaxation patterns is better and does not die out with a distance increase (at least up to 400 Å).[6]

In line with these experimental reports, in our modelling we see the following:

•We observed a well developed C-type Va order for $x_{\mathrm{Gd}} \gtrsim 0.4$–$0.5$, as $Y(\mathrm{O2})$ approaches the $1 - x_{\mathrm{Gd}}$ limit. Oxygen vacancies are spread over the whole MC supercell (random configuration of cations).

•As mentioned, misorientation angles are much smaller for $x_{\mathrm{Gd}} = 0.75$ than for $x_{\mathrm{Gd}} = 0.50$.

These results qualitatively agree with reported, as one can expect a good spatial alignment of C-phase domains for well developed C-type order and small misorientation angles.

References

1 P. A. Žguns, A. V. Ruban and N. V. Skorodumova, *Phys. Chem. Chem. Phys.*, 2017, **19**, 26606–26620.

2 C. Artini, M. Pani, A. Lausi, R. Masini and G. A. Costa, *Inorg. Chem.*, 2014, **53**, 10140–10149.

3 M. Scavini, M. Coduri, M. Allieta, M. Brunelli and C. Ferrero, *Chem. Mater.*, 2012, **24**, 1338–1345.

4 M. Coduri, M. Scavini, M. Pani, M. M. Carnasciali, H. Klein and C. Artini, *Phys. Chem. Chem. Phys.*, 2017, **19**, 11612–11630.

5 C. Artini, M. Pani, M. M. Carnasciali, M. T. Buscaglia, J. R. Plaisier and G. A. Costa, *Inorg. Chem.*

6 M. Scavini, M. Coduri, M. Allieta, P. Masala, S. Cappelli, C. Oliva, M. Brunelli, F. Orsini and C. Ferrero, *IUCrJ*, 2015, **2**, 511–522.